Experimentální Analýza Napětí 2007

X-RAY DIFFRACTION STUDY OF RESIDUAL STRESS DISTRIBUTION DUE TO MILLING OF STEELS

Kamil Kolařík[1], Nikolaj Ganev,[2] Pavel Zeman [3], Totka Bakalova[4]

Abstract: *The aim of this paper is to study the depth profiles of macroscopic residual stresses in surface layers of steel samples milled with carbide-tipped tools. The impact of five different ways of cooling during milling was investigated. Oil emulsion, aerosol of air and oil, and cooled and frozen air from a Ranque-Hilsch vortex tube were used as coolants. The state of residual stresses was studied in two directions by means of the X-ray diffraction technique. Considering that the penetration depth of CrKα X-ray radiation in steels is less than 5 μm, electrochemical etching was applied for surface layer removal up to 0.21 mm.*

Keywords: *residual stresses, X-ray diffraction, milling, impact of cooling*

1. Introduction

Progress in technology has always been accompanied by increasing demands on construction of machine components, in particular in automotive and aeronautics industries as well as in nuclear power-plant engineering. The growing requirements for safety and reliability of these products and their parts are closely related to technological procedures in manufacturing and final treatment. New high-strength materials and high rates of reduction during final surface creation raise misgivings about a favourable impact of the great energy put in the surface on functional properties of machine parts. New progressive manufacturing techniques include precise formation of intermediate (precision casting, shaping, etc.) and follow-up progressive methods for creating the final surface. High-speed cutting (HSC) including its modifications called “dry” or “hard” machining and chipless working (e.g., EDM – electro discharge machining, LBM – laser beam machining, ECM – electrochemical cutting) definitely belong to new progressive techniques for final surface creation.

Residual stresses represent one of the most important attributes of surface layers. If the residual stresses are known, it will be possible to predict operational reliability of mechanical parts and choose such surface treatment that results in creating a compressive pre-stressed layer acting as a barrier to prevent crack propagation into the material.

Economical production procedures for manufacturing of complex-shaped surfaces like moulds´ and dies´ cavities, holes of shearing and working tools, shaping surface of steam and gas turbines and jet engines, etc. require a thoroughgoing choice of a proper progressive machining technique. HSC methods carried out on the basis of CAD models enable direct

[1] Ing. Kamil Kolařík, KIPL FJFI ČVUT v Praze, Trojanova 13, 120 00 Praha 2, tel.: +420 224 358 624, e-mail: kamil.kolarik@email.cz

[2] Doc. Ing. Nikolaj Ganev, CSc., KIPL FJFI ČVUT v Praze, Trojanova 13, 120 00 Praha 2 tel.: +420 224 358 604, e-mail: ganev@troja.fjfi.cvut.cz

[3] Ing. Pavel Zeman, Ph.D., VCST, FS ČVUT v Praze, Horská 3, 128 00 Praha, tel.: +420 221 990 923, e-mail: p.zeman@rcmt.cvut.cz

[4] Ing. Totka Bakalova, TU v Liberci, FS, Katedra obrábění a montáže, Hálkova 6, 461 17 Liberec, e-mail: tbakalova@abv.bg

milling of quenched high-strength materials of hardness up to 58 HRC when ultimate strength is less than 2 000 MPa. The main asset of high-speed cutting is the quality of the treated surface that often does not require finishing. The distribution of residual stresses in surface layers is not usually taken into account in manufacturing technology design.

2. Samples investigated

The effect of a cutting environment on residual stresses in a machined surface layer was studied on the end milled steel of Czech grade 12 050.9 at six different cutting environments. Samples of dimensions 50×15×7 mm^3 were labelled ***A, B, C, D, E,*** and ***F***. Working and cutting conditions were the same for all of them. A variance occurred in the cutting environment only. All the working and cutting conditions are outlined in Tab.1. A unique experimental milling machine tool LM-2 (Fig.1) with linear drives was used in the experiments. Milling was carried out using the coated hard metal tool tips. The schematic diagram of the cutting operation is shown in Fig 2.

Working conditions	type of the tool	end mill
	tool diameter D_n [mm]	20
	number of tool teeth [-]	3
	insert type	APKX 11
	tool material	ISO P25-40
	tool coating	multi TiN (TiAlSi)N
	cutting operation	down-milling
	workpiece material	12050.9
	machine tool	LM-2
Cutting conditions	cutting speed v_c [m.min^{-1}]	210
	feed per tooth f_z [mm]	0,15
	axial depth of cut a_p [mm]	2
	radial depth of cut a_e [mm]	16

Tab. 1. Working and cutting conditions used in the experiments

Fig.1. LM-2 machine tool.

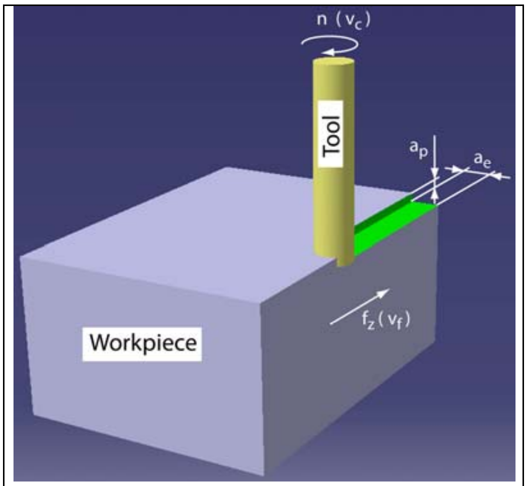

Fig.2 Schematic diagram of the cutting operation.

The specification of particular cutting environments is as follows. First, cutting was made in a natural environment (Fig. 3a) – sample ***A***. Flood cooling of the cutting tool with oil emulsion was applied in next two experiments. External cooling by two nozzles (sample ***B***) is shown in Fig. 3b. Internal cooling through the spindle and the tool (sample ***C***) was used in the third experiment (Fig. 3c). The concentration of the oil emulsion (water + Ecocool 2520) was 5 %. A more ecological way of cooling and lubricating than in the previous cutting environment is a minimum quantity lubrication (MQL). Aerosol of air and oil was applied to the cutting region by two external nozzles in this case (Fig. 3d) – sample ***D***. The cutting environments with cooled (+4°C) and frozen (-8°C) compressed air (samples ***E*** and ***F***) were produced using a vortex tube. The air was applied by one external nozzle (Fig. 3e).

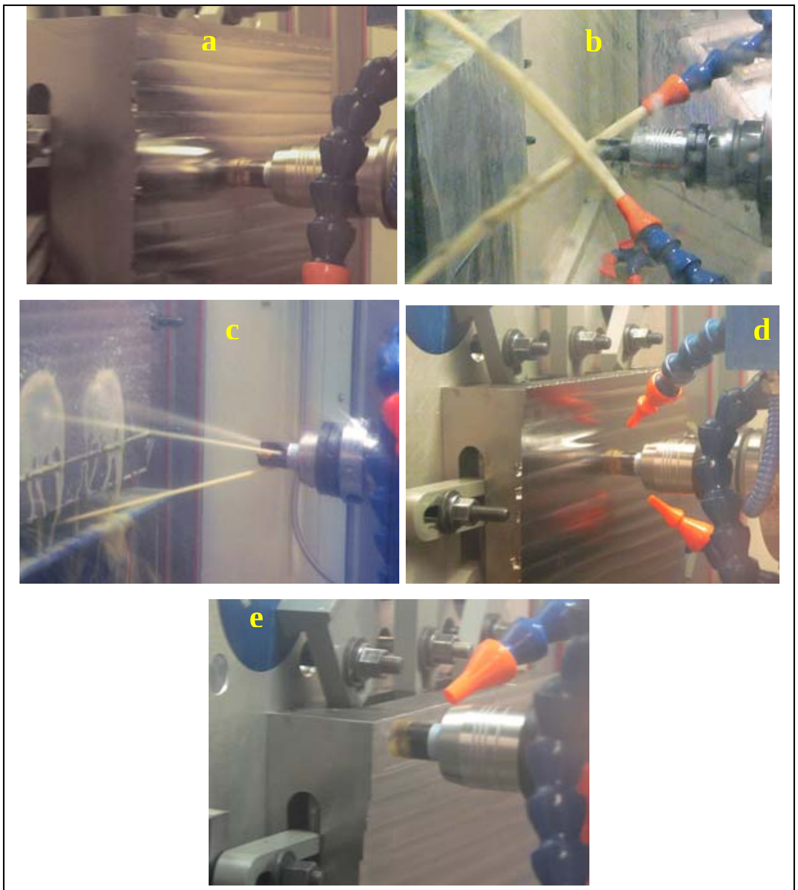

Fig.3. Various cutting environments

3. Experimental

3.1 X-ray diffraction technique

The "one-tilt" method with no reference substance (Fig. 4) was applied to find residual stresses by the X-ray method [1]. The incident CrKα beam directed by a cylindrical collimator of 1.7 mm in diameter reached the sample surface 50×15 mm^2 at an angle of ψ_0 = 45° in the longitudinal and transversal direction, in which the surface components of stress σ_L and σ_T, respectively, were analyzed. The record of the {211} α-Fe diffraction line intensity curve was obtained from a position sensitive detector based on imaging plates (Fig. 5). In the case of this experimental arrangement, the surface stress σ_φ can be written as

$$\sigma_\varphi = \frac{1}{½ s_2} \frac{\operatorname{cotg}\theta . \cos^2 2\theta}{2D} \frac{\Delta^{hkl}}{\sin 2\eta}, \tag{1}$$

where θ is the Bragg angle, η = 90º – θ, D is the distance between the film and the sample, and $\Delta^{hkl} = r_{\psi_1} - r_{\psi_2}$ is the eccentricity of the diffraction ring [2]. The X-ray elastic constant $½s_2 = 5.76 \cdot 10^{-6}\ N^{-1}m^2$ was used in residual stress calculations. The experimental inaccuracy does not exceed 40 MPa.

Fig. 4. Experimental arrangement for the X-ray diffraction "one-tilt" method

3.2 Determination of residual stress depth profile

Due to the limitations of X-ray penetration depth, the X-ray diffraction technique can be used only for surface layers few micrometers in thickness.

In the case of conventional X-ray diffraction apparatus, investigation of stress depth profiles is performed in combination with electrochemical etching. The process of anodic dissolution takes place during electrochemical etching while the anode is formed by the sample itself; the product of this process is a solution of high electrical resistance which is embedded into microscopic wells in the surface of the sample and, therefore, preferential removal of roughness proceeds.

The ***LectroPol-5*** by ***Struers***, a device for automatic micro-processor controlled electrolytic polishing and etching of metallographic specimen was used for surface layer removal. An area of 14 mm in diameter was gradually subject to electrolytic polishing and residual stresses were analysed.

Fig. 5. Evaluation of diffraction patterns detected with a position sensitive detector based on imaging plates

4. Results and their discussion

The results of X-ray diffraction analysis of macroscopic residual stresses obtained after gradual etching of the surface as well as the average value of width of the {211} diffraction line, which could be interpreted as a degree of plastic deformation of the crystal lattice, are shown in Tables 2 – 7. The obtained depth profiles are illustrated in Figures 6 – 11.

z, mm	**σ_L, MPa**	**σ_T, MPa**	**W, °**
0,00	197	374	1,95
0,01	-194	79	1,76
0,02	-169	-44	1,64
0,04	-289	-126	1,51
0,08	-310	-84	1,35
0,12	-277	-25	1,21
0,16	-76	-41	1,11
0,21	-76	-43	1,13

Tab. 2 Macroscopic residual stresses in longitudinal ($\boldsymbol{\sigma_L}$) and transversal ($\boldsymbol{\sigma_T}$) directions and the average value of the width of the {211} diffraction line obtained for different depths (***z***) for sample ***A***

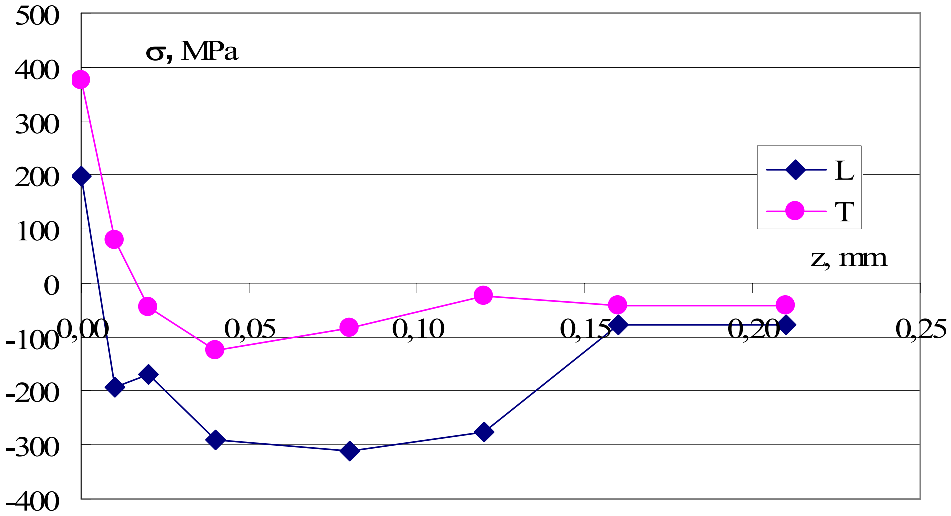

Fig. 6. Depth distribution of residual stresses σ_L (L) and σ_T (T) obtained for sample ***A***

z, mm	σ_L, MPa	σ_T, MPa	W, °
0,00	136	448	1,99
0,01	-125	42	1,70
0,02	-234	-25	1,60
0,04	-266	-93	1,50
0,08	-295	-110	1,32
0,12	-110	-101	1,20
0,16	-97	-47	1,10
0,21	-24	13	1,14

Tab. 3 Macroscopic residual stresses in longitudinal (σ_L) and transversal (σ_T) directions and the average value of the width of the {211} diffraction line obtained for different depths (z) for sample ***B***

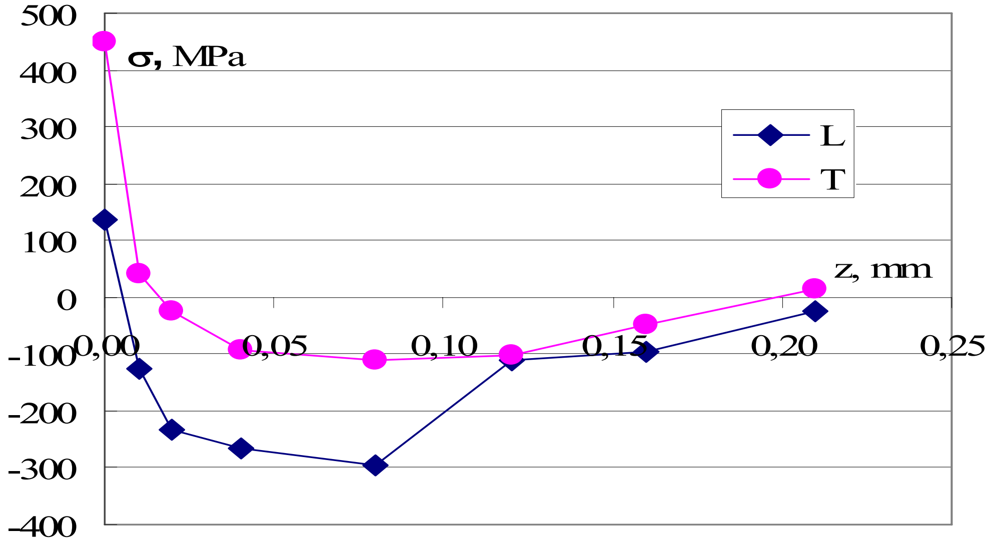

Fig. 7. Depth distribution of residual stresses σ_L (L) and σ_T (T) obtained for sample ***B***

z, mm	σ_L, MPa	σ_T, MPa	W, °
0,00	317	465	1,98
0,01	-123	141	1,68
0,02	-225	30	1,64
0,04	-339	-43	1,50
0,08	-315	-71	1,32
0,12	-118	-39	1,27
0,16	-120	85	1,18
0,21	-45	109	1,12

Tab. 4 Macroscopic residual stresses in longitudinal (σ_L) and transversal (σ_T) directions and the average value of the width of the {211} diffraction line obtained for different depths (z) for sample ***C***

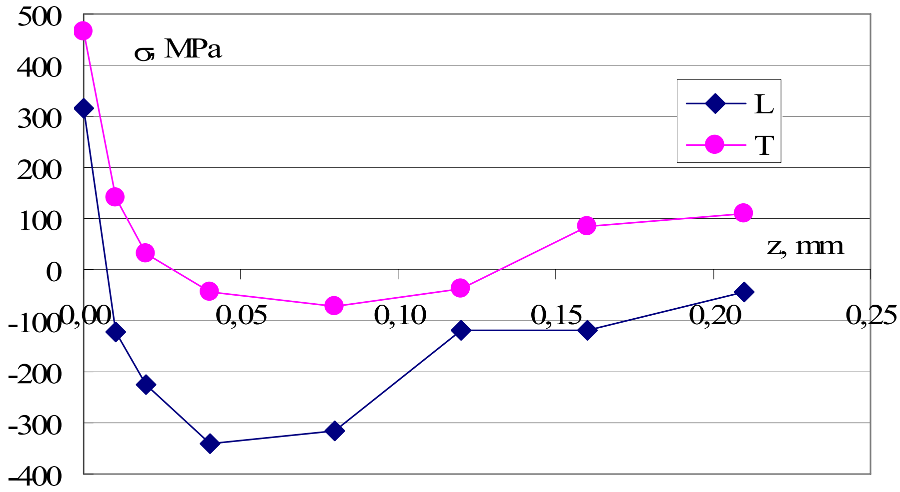

Fig. 8. Depth distribution of residual stresses $\boldsymbol{\sigma_L}$ (L) and $\boldsymbol{\sigma_T}$ (T) obtained for sample ***C***

z, mm	**σ_L, MPa**	**σ_T, MPa**	**W, °**
0,00	335	339	2,00
0,01	-86	170	1,76
0,02	-241	143	1,68
0,04	-281	9	1,48
0,08	-229	-64	1,33
0,12	-123	-26	1,24
0,17	-67	11	1,14
0,21	-8	-34	1,12

Tab. 5 Macroscopic residual stresses in longitudinal ($\boldsymbol{\sigma_L}$) and transversal ($\boldsymbol{\sigma_T}$) directions and the average value of the width of the {211} diffraction line obtained for different depths ($\boldsymbol{z}$) for sample ***D***

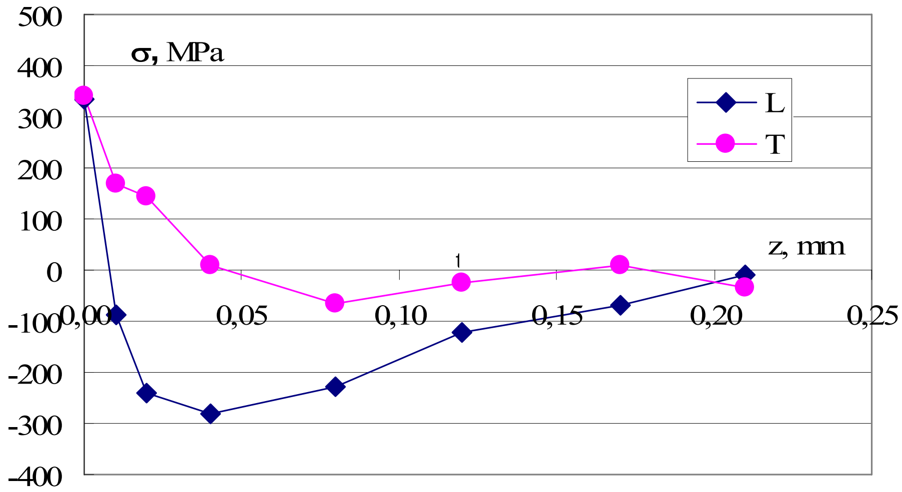

Fig. 9. Depth distribution of residual stresses σ_L (L) and σ_T (T) obtained for sample ***D***

z, mm	σ_L, MPa	σ_T, MPa	W, °
0,00	249	218	1,96
0,01	-184	92	1,71
0,02	-198	-17	1,65
0,04	-309	-12	1,46
0,08	-196	-6	1,34
0,12	-132	-2	1,18
0,17	-44	54	1,12
0,21	-7	46	1,12

Tab. 6 Macroscopic residual stresses in longitudinal (σ_L) and transversal (σ_T) directions and the average value of the width of the {211} diffraction line obtained for different depths (*z*) for sample ***E***

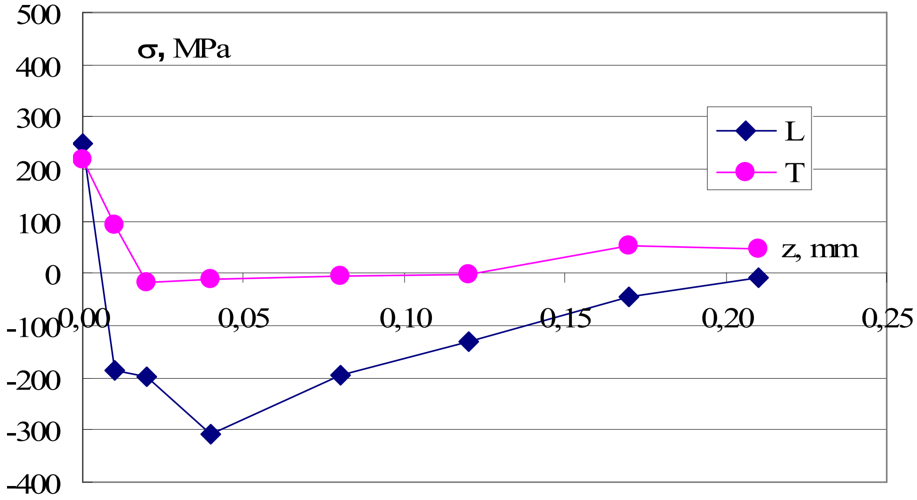

Fig. 10. Depth distribution of residual stresses σ_L (L) and σ_T (T) obtained for sample ***E***

z, mm	**σ_L, MPa**	**σ_T, MPa**	**W, °**
0,00	246	235	1,94
0,01	-149	52	1,70
0,03	-182	-45	1,63
0,05	-287	-71	1,48
0,08	-181	-10	1,34
0,12	-208	-46	1,20
0,17	-52	-37	1,19
0,21	-15	68	1,12

Tab. 7 Macroscopic residual stresses in longitudinal (σ_L) and transversal (σ_T) directions and the average value of the width of the {211} diffraction line obtained for different depths (z) for sample ***F***

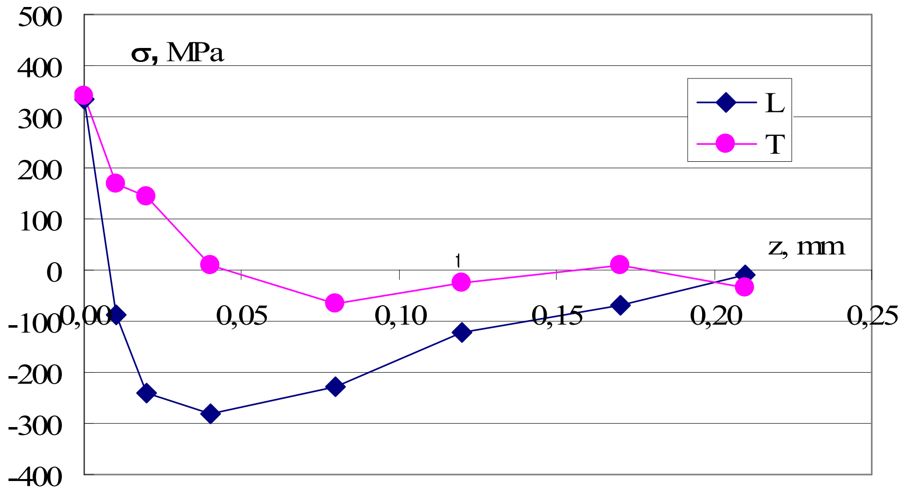

Fig. 11. Depth distribution of residual stresses σ_L (L) and σ_T (T) obtained for sample ***F***

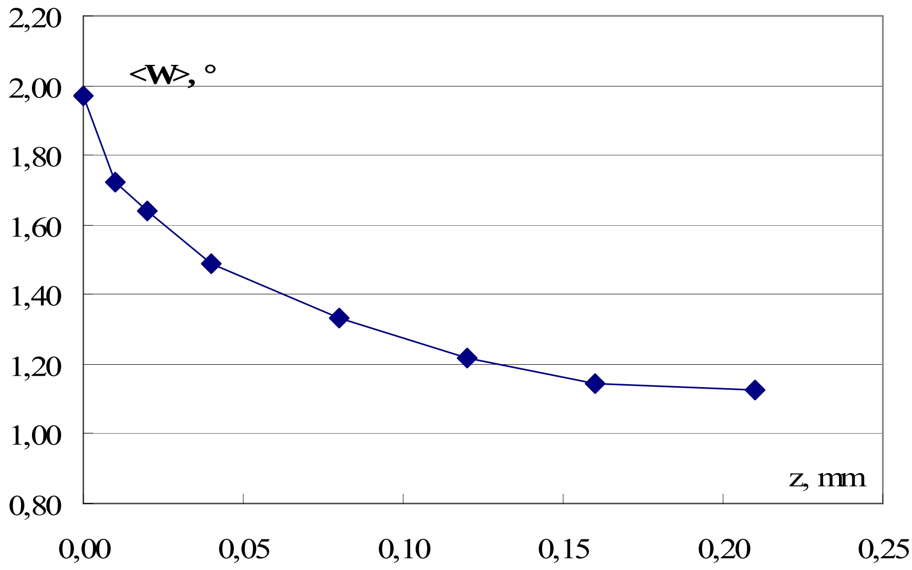

Fig. 12. Average width of the {211} diffraction line obtained for all the investigated samples

As can be seen from Figures 6 – 11, courses of the obtained longitudinal σ_L and transversal σ_T stresses for all the investigated samples ***A, B, C, …, F*** have the same character beneath the treated surface. In order to interpret the obtained experimental data from the point of view of different cooling conditions and, thus, to distinguish the impact of applied cutting environments, the follow-up discussion will focus on the behaviour of induced residual stresses on the surface and instantly beneath the surface. These characteristics are summed up in Tab. 8.

Sample	A	B	C	D	E	F
σ_{Ls}, **MPa**	197	136	317	335	249	246
σ_{Ts}, **MPa**	374	448	465	339	218	235
g_L, **MPa.μm**$^{-1}$	39,1	26,1	44	42,1	43,3	39,5
g_T, **MPa.μm**$^{-1}$	29,5	40,1	32,4	16,9	12,6	18,3

Tab. 8. Surface residual stresses σ_{Ls}, σ_{Ts} and their subsurface gradients g_L, g_T calculated using the first two pairs (z, σ) from Tables 2 – 7.

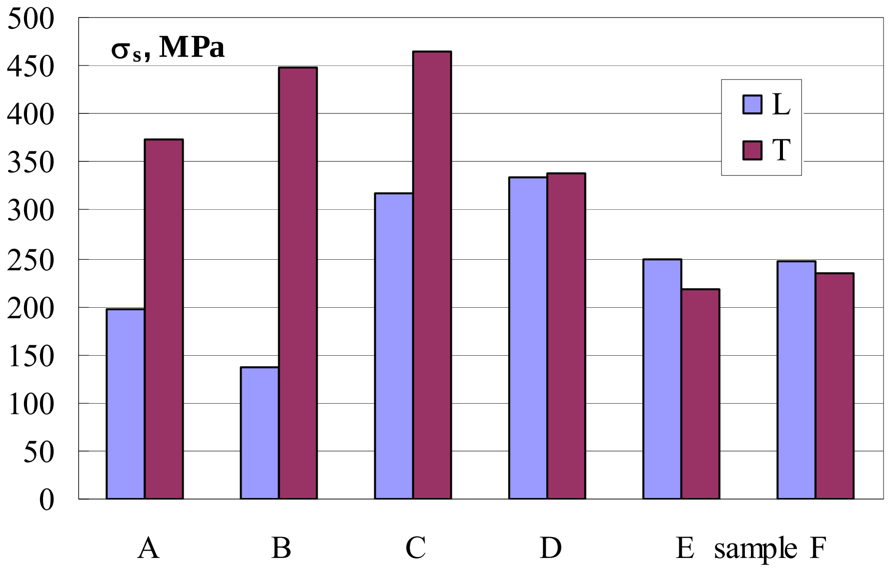

Fig. 13. Residual stresses measured in longitudinal ***L*** (σ_{Ls}) and transversal ***T*** (σ_{Ts}) direction on the surface of analysed samples

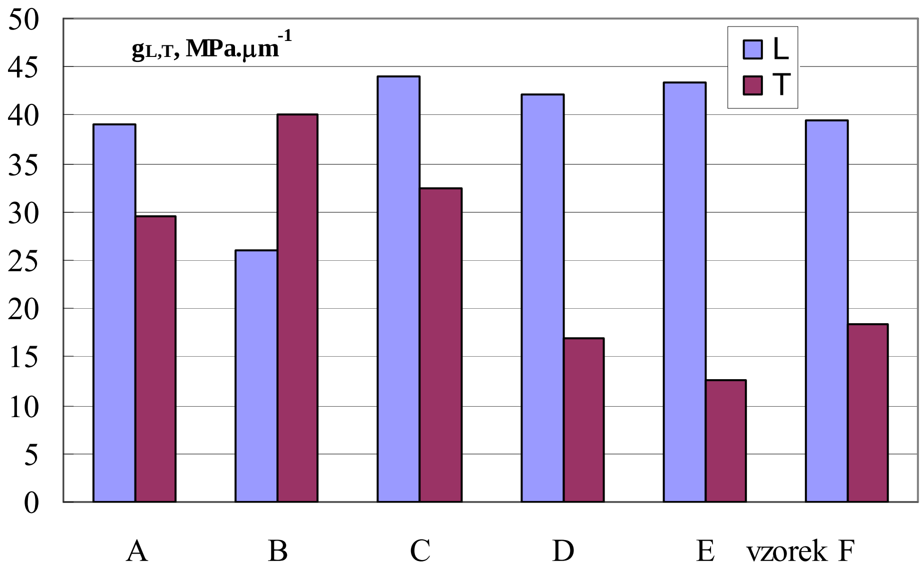

Fig. 14. Subsurface gradients g_L (***L***) and g_T (***T***) in both the directions of measurement

5. Conclusions

The performed X-ray diffraction analysis enables to make the following conclusions about the effect of cutting environment on residual stresses in surface layers of milled steel 12 050.9:

- Residual stress (RS) profiles for depths of z > 0.010 mm are analogous for all the investigated samples and do not vary substantially with cooling conditions.
- The state of RS in depths of z > 0.010 mm is anisotropic and longitudinal stresses are systematically lower than the transversal ones, i.e. $\sigma_L < \sigma_T$, which, in all probability, is a consequence of the asymmetry of cutting.
- The course of the width of the {211} diffraction line obtained for all the investigated samples (Tab. 12) indicates that the thickness of the plastically deformed surface layer is approx. 0.15 – 0.20 mm. This finding corresponds with the character of RS distributions (see Figs. 6 – 11) where the values of RS at a depth of 0.15 – 0.20 mm are not significant.
- The main impact of various cutting environments could be observed on the behaviour of residual stresses obtained on the surface and instantly beneath it for $z \leq 0.010$ mm, see Tab. 8, Figs. 13 – 14.
- All the obtained surface RS are tensile. While the surface state of RS in the case of samples ***A***, ***B,*** and ***C*** is anisotropic ($\sigma_L < \sigma_T$), cooling conditions of ***D***, ***E*** and ***F*** (aerosol of air and oil, and compressed cold air) lead to an isotropic stress field ($\sigma_L \approx \sigma_T$). Moreover, surface tensile values on samples ***E*** and ***F*** are the lowest as a whole.
- Subsurface gradients (calculated using the first two pairs (z, σ) from Tables 2 – 7) of longitudinal stresses g_L are higher than g_T with an exception of sample ***B*** (Fig. 14).
- Samples ***D***, ***E,*** and ***F*** show higher “gradients’ anisotropy” in comparison with the other three samples, i.e., g_L for them is more than twice as great as g_T.

Acknowledgements: The research has been supported by the Projects MSM 6840770021 and No. 1M0507 of the Ministry of Education, Youth and Sport of the Czech Republic.

References

[1] Kraus I., Ganev N.: Technické aplikace difrakční analýzy, Vydavatelství ČVUT, Praha 2004.

[2] Ganev N., Kraus I.: Čs.čas.fyz. A36, 1986, 270.